JOURNAL OF GEOPHYSICAL RESEARCH, VOL. 112, E06010, doi:10.1029/2006JE002869, 2007

Deposition and degradation of a volatile-rich layer in Utopia Planitia and implications for climate history on Mars

Anne Morgenstern,[1,2] Ernst Hauber,[2] Dennis Reiss,[2,3] Stephan van Gasselt,[4] Guido Grosse,[5] and Lutz Schirrmeister[1]

Received 28 November 2006; revised 27 February 2007; accepted 7 March 2007; published 28 June 2007.

[1] We investigate the surface morphology of a study area in western Utopia Planitia, Mars, which is characterized by a variety of landforms that resemble those of terrestrial periglacial landscapes. Polygonally fractured ground and thermokarst-like depressions are found to be located in a young mantling deposit with a thickness of several tens of meters. We observe a latitudinal dependence of the degradation of this mantling deposit. Larger depressions, whose floors reveal the underlying basement rocks, cover a higher fraction of the total terrain in the southern part of the study area than in the northern part, indicating a more intense degradation of the mantle in the south. All depressions have an asymmetric cross section in north-south direction, interpreted to be the result of the different solar radiation on differently oriented slopes. On the basis of our morphological observations, we develop a conceptual model for landscape evolution in western Utopia Planitia. It involves subaerial deposition of a layered, ice-rich mantle and its subsequent degradation by polygon formation and sublimation. A terrestrial analog to the polygonally fractured mantling deposit and its thermokarst-like depressions is the Siberian Ice Complex or "Yedoma," which consists of subaerial ice-rich deposits and is connected to nonglaciated landscapes with highly continental cold-climatic environmental conditions. Our comparison suggests that no unusual or exotic processes need to be invoked to explain the current morphology of western Utopia. However, the young age of the deposition and degradation implies climatic excursions in the very recent past on Mars.

Citation: Morgenstern, A., E. Hauber, D. Reiss, S. van Gasselt, G. Grosse, and L. Schirrmeister (2007), Deposition and degradation of a volatile-rich layer in Utopia Planitia and implications for climate history on Mars, *J. Geophys. Res.*, *112*, E06010, doi:10.1029/2006JE002869.

1. Introduction

[2] The degradation of ice-bearing permafrost deposits on Earth is predominantly connected to externally forced changes in the thermo-physical range of permafrost stability at the land surface. Major forcing factors are climate warming and the disturbance or removal of insulating cover layers. Both can result in a deepening of the seasonal active layer, the melting of ground ice along with volume loss, and surface subsidence. By analogy, the investigation of permafrost degradation (i.e., thermokarst) on Mars can provide important information about changes in the environmental conditions affecting the planet's surface processes.

[3] Possible thermokarst features on Mars were first suggested from Mariner 9 imagery by *Sharp* [1973], which show similarities to terrestrial thermokarst terrains in Alaska that formed in unconsolidated sediments with variable ice content [*Gatto and Anderson*, 1975]. Viking Orbiter images with higher spatial resolution revealed that these features are similar in size and shape to terrestrial thermokarst. These features are not ubiquitous on Mars, but are concentrated in specific regions such as Chryse Planitia [*Carr and Schaber*, 1977; *Theilig and Greeley*, 1979], Utopia and Acidalia Planitiae [*Costard and Kargel*, 1995], and the Argyre basin [*Kargel and Strom*, 1992]. The occurrence of thermokarst in these regions may be due to degradation of ice-rich sedimentary deposits in the near-subsurface originating from flooding of the outflow channels [*Costard and Kargel*, 1995; *Costard and Baker*, 2001], and from possible ancient lakes [*Kargel and Strom*, 1992]. *Lucchitta* [1985] suggests that discrete ice lenses within the Martian surface material could enhance the efficiency of thermokarst development.

[4] Small-scale polygonal fracture patterns that are attributed to thermal contraction cracking of the upper surface layer are common features on Mars and have been first observed in Viking Lander and high-resolution Orbiter

[1]Alfred Wegener Institute for Polar and Marine Research, Research Unit Potsdam, Potsdam, Germany.
[2]Institute of Planetary Research, German Aerospace Center (DLR), Berlin, Germany.
[3]Institut für Planetologie, Westfälische Wilhelms-Universität Münster, Münster, Germany.
[4]Institute for Geosciences, Free University Berlin, Berlin, Germany.
[5]Geophysical Institute, University of Alaska Fairbanks, Fairbanks, Alaska, USA.

0148-0227/07/2006JE002869$09.00

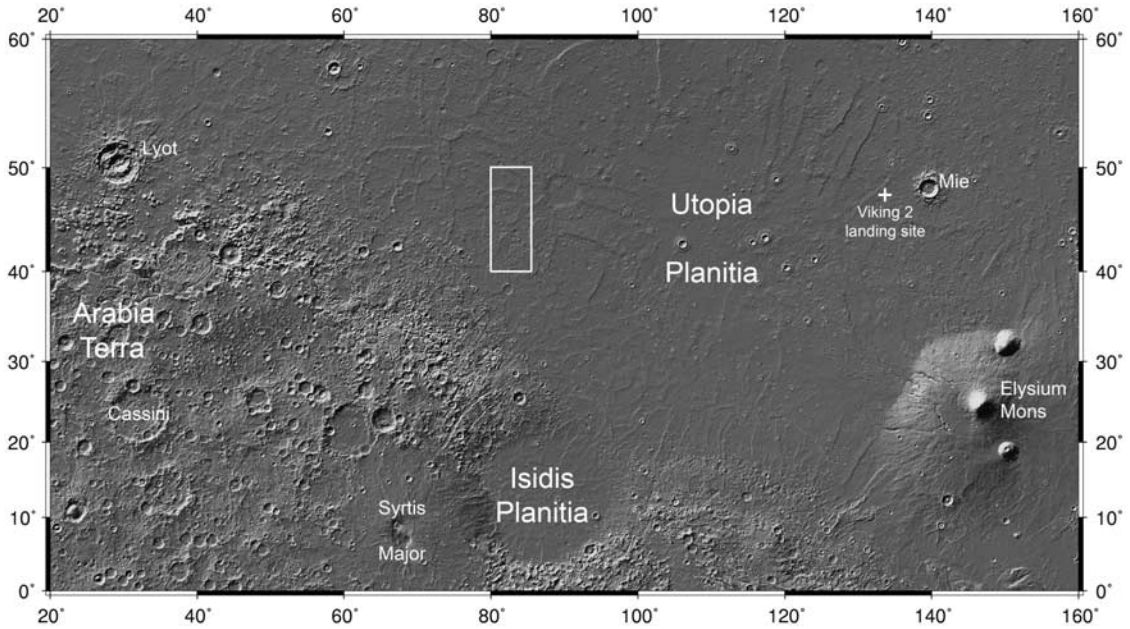

Figure 1. Location of the study region (white box).

image data [*Mutch et al.*, 1977; *Lucchitta*, 1981, 1983; *Kuzmin*, 1983]. These Martian landforms have been interpreted as possible ice-wedge polygons [*Mutch et al.*, 1977; *Lucchitta*, 1981] that do not only require single events of cracking as controlled by surface temperature gradients, but also growing of cracks through thaw-freeze cycles of the uppermost layer.

[5] Detailed characterizations on the basis of high-resolution data of the Mars Global Surveyor Mars Orbiter Camera–Near Angle (MGS MOC–NA) telescope have been performed by a variety of authors [*Yoshikawa*, 2000, 2003; *Seibert and Kargel*, 2001; *Kuzmin et al.*, 2002; *Mangold et al.*, 2004; *van Gasselt et al.*, 2005] in the recent past. Although a consistent view on the global distribution of these features has not been provided yet, it can be roughly stated that these fracture patterns are restricted mainly to two latitude bands, one located between 40–50° to 80°N with a dense distribution around 60°N and the other one located between 50° to 90°S with a dense occurrence of fracture patterns around 70°S [*Seibert and Kargel*, 2001; *Kuzmin and Zabalueva*, 2003; *Mangold et al.*, 2004]. While the north-polar area seems to be in lack of any of these fracture patterns, the south-polar area shows an abundant variety of such landforms of different shapes and sizes [*Kossacki and Markiewicz*, 2002; *Piqueux et al.*, 2003; *van Gasselt et al.*, 2003, 2005]. The midlatitude distribution corresponds generally to the distribution of permafrost related morphologies [*Squyres*, 1978, 1979; *Squyres and Carr*, 1986; *Squyres et al.*, 1992] and theoretical predictions of the depth of permafrost [*Zent et al.*, 1986; *Paige*, 1992; *Mellon*, 1997].

[6] In contrast to the so-called giant polygons on Mars that are predominantly restricted to the northern lowlands of the circum-Utopia region, and which have a size of several kilometers, and are attributed to tectonic processes and sediment-loading effects [*Hiesinger and Head*, 2000], small-scaled features have a diameter-size range of 20–300 m [*Seibert and Kargel*, 2001; *Yoshikawa*, 2000; *Kuzmin et al.*, 2002; *van Gasselt et al.*, 2003] and are quite similar to their terrestrial counterparts [*Lachenbruch*, 1962, 1966; *Black*, 1976; *French*, 1996; *Yershov*, 2004].

[7] We investigate a region of about 122,000 km^2 in western Utopia Planitia, extending from about 80° to 85°E and from 40° to 50°N (Figure 1). Recent mapping by *Tanaka et al.* [2005] identified two surface units within the study area: Unit ABa covers the southern two thirds of the area (up to ~47.5°N). It is interpreted as a volatile-rich mantling unit of Late Amazonian age, which overlies the Utopia Planitia and Vastitas Borealis units with a thickness of a few tens of meters. This mantle was recognized on the basis of MOLA topographic data [*Kreslavsky and Head*, 2000] and MOC images [e.g., *Mustard et al.*, 2001], although hints to such a mantle were already observed in Mariner 9 data from the presence of an eolian mantle at high latitudes [*Soderblom et al.*, 1973] and in Viking Orbiter images from latitude-dependent ''terrain softening'' [*Squyres and Carr*, 1986]. In the northern third of the study area, *Tanaka et al.* [2005] mapped the unit ABvi (Vastitas Borealis Interior Unit) and interpreted it as Early Amazonian sediments of the outflow channels, e.g., a sublimation residue from frozen ponded bodies of water [*Kreslavsky and Head*, 2002]. Several morphological features like polygonally dissected terrain and pits or depressions in the mantling deposit show close similarities to terrestrial permafrost structures. Their origin has been attributed to periglacial processes and permafrost degradation [e.g., *Seibert and Kargel*, 2001; *Kuzmin and Zabalueva*, 2003; *Mangold*, 2005; *Soare et al.*, 2005a], but aeolian processes [*Soare et al.*, 2005b] and structural control [*Yoshikawa*, 2003] have also been suggested. Our focus is on degradation features and their formation, and we compare the observations with our own field experience in Arctic Siberia as terrestrial reference [*Grosse et al.*, 2005, 2006, 2007].

[8] Although a permafrost-related origin is assumed for these small-scaled polygonal patterns, any observational evidence is still missing. Modeling attempts as conducted by [*Mellon*, 1997] have shown that tensile stresses caused

by variations of surface temperatures easily exceed the tensile strength of the Martian regolith in areas north and south of 20°–30° supporting formation of contraction cracks. Missing subsurface hydrogen abundance as derived from measurements of the Neutron Spectrometer instrument on board Mars Odyssey suggest that the formation of these landforms is controlled by the climatic environment and that they may have been shaped through sublimation processes [*Mangold et al.*, 2004] .

2. Permafrost Degradation and Thermokarst on Earth

[9] Terrestrial permafrost is defined as any ground that remains ≤0°C for at least two consecutive years [*van Everdingen*, 2005]. According to this definition about 24% of the Earth's northern hemisphere land surface are influenced by permafrost [*Zhang et al.*, 1999]. Permafrost on Earth is predominantly distributed between 55–75° northern latitude. Other important permafrost regions are found in the high mountains (e.g., Tibetan Plateau), and in ice-free oases of Antarctica (e.g., Dry Valleys). Terrestrial permafrost started to form during the Late Cenozoic global cooling about 2.5 million years ago. The most extensive distribution and thickness (up to 1500 m) are found in eastern Siberia, where stable dry and cold climate conditions persisted for a comparatively long time period. Depending on the latitude, the temperature of Siberian permafrost varies between −12°C in the north and 0°C at the southern permafrost boundary. Varying ice contents are known from terrestrial permafrost regions. The highest ice contents are usually found in fine-grained silty to sandy sediments of aeolian, alluvial or proluvial origin, where they can reach 50–90% by volume. The ground ice occurs as large ice wedges, forming polygonal nets at the terrain surface and wedge like ice structures in the sediments, and segregated ground ice, forming small ice lenses and subhorizontal ice bands in the sediments. Due to the high ice content, such deposits are prone to massive geomorphological change during periods of climatic warming. The most important terrestrial permafrost degrading process, thermokarst, describes the loss of ground ice without the activity of running water. It is defined as the thawing of ice-rich permafrost or the melting of massive ice in the subsurface [*van Everdingen*, 2005]. Thermokarst results in surface subsidence and the formation of characteristic, mostly circular depressions due to the volume loss from ground ice melting (Figures 2a and 2b). Widespread thermokarst is thus a clear climate signal.

[10] A thermokarst depression deepens as long as the surface energy input is sufficient to produce a downward migrating melting front through ice-bearing sediments. In a later stage, the ground ice depleted surface material in a thermokarst depression may form an insulating cover preventing this downward migration of the melting front and

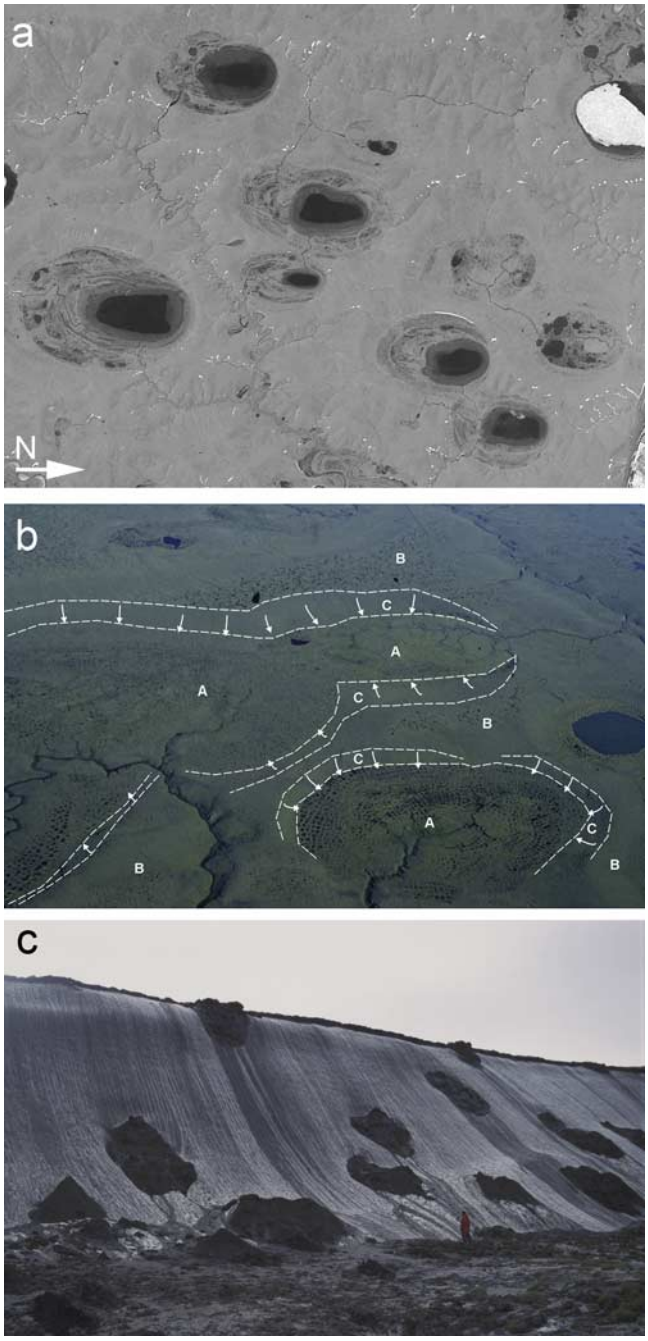

Figure 2. Suggested terrestrial analog for a degrading volatile-rich frozen mantle deposit: Three examples of landscapes underlain by ice-rich fine grained deposits (Yedoma) indicating strong influence of permafrost degradation (thermokarst). (a) CORONA image of circular thermokarst depressions of 20–30 m depth in ice-rich permafrost deposits in the Lena-Anabar lowland, NE Siberia. Subaerial parts of the depressions display terracing and polygonal ice wedge nets. The lakes have diameters between 500 m and 1000 m. (b) Air photo of thermokarst depressions in the Yana-Indigirka lowland (July 1999) (A, basin floors; B, surrounding uplands; C, slopes). The small depression has a diameter of 300 m. (c) Thermoerosive outcrop at Oyagoss Yar lowland, NE Siberia, with ice-rich permafrost deposits showing large ice-wedges (light gray) and frozen soils (Ice Complex) (dark gray-black). Soils outcropping on the cliff are in situ and still frozen (= soils within the ice wedge polygons); black material on the floor is thawed soil originating from the receding cliff and was transported by slumping (photo: G. Grosse).

thus further deepening. Lateral growth of a basin due to thermoerosion along the slopes and gravimetric mass wasting can result in the coalescence with neighboring basins. Long-term regular or irregular cycles of thawing and refreezing over several 1000 years may result in the repeated formation and melting of ground ice in the already existing basins. This process can result in the formation of complicated nested thermokarst basins, which is the case, e.g., for the Alaskan Northslope region [e.g., *Hinkel et al.*, 2003]. Thermokarst depressions have characteristic morphological features like steep slopes and often also terraces, reflecting rapid or gradual subsidence, respectively. The bottoms of the depressions are generally plain and very often display polygonal patterns caused by ice wedge growth in a refreezing basin (Figure 2b). The rims of the depressions are usually cut by numerous small valley systems formed by thermoerosion.

[11] The vast thermokarst-dominated landscapes in the NE Siberian lowlands are a result of the warmer and moister climatic conditions during the Early Holocene climate warming ~11,500 years ago [e.g., *Grosse et al.*, 2007]. During that period large parts of the permafrost became unstable and the permafrost boundary shifted northward, initiating widespread permafrost degradation especially in ice-rich ground. In the previous glacial period of the Late Pleistocene (~100,000 – 11,500 years ago) permafrost aggradation in the northern hemisphere resulted in permafrost thickening and a southward shift of the permafrost boundary. In addition to aggradation, extensive 10–60 m thick ice-rich deposits accumulated in large parts of the Arctic lowlands in NE Siberia [e.g., *Schirrmeister et al.*, 2002]. This so-called Ice Complex or "Yedoma" consists of mostly fine-grained subaerial deposits of different facies (polygenetic) and its formation is connected to nonglaciated landscapes with highly continental cold-climatic environmental conditions with large seasonal temperature differences and small annual precipitation. The Yedoma is characterized especially by its high ground-ice contents of 50 to 80 vol-% and the presence of large ice wedges that grew over several 10,000 years to dimensions of up to 40 m length and 5–8 m width (Figure 2c). Thermokarst in ice-rich Yedoma expresses as large and partly coalesced basins with up to 40 m depth and several km width. According to remote sensing calculations about 50% of the Yedoma areas in the Siberian Laptev Sea lowlands are characterized by thermokarst depressions, and up to 80% of the area shows signs of permafrost degradation [*Grosse et al.*, 2006].

[12] On Earth, thermokarst formation is strongly interacting with the hydrological regime, often resulting in thermokarst lakes that enhance the permafrost thawing and subsidence.

3. Methods

[13] We used High Resolution Stereo Camera (HRSC) and Thermal Emission Imaging System Visible (THEMIS-VIS) images as a base for manually digitizing depressions in the mantling deposit attributable to permafrost degradation in a geoinformation system GIS (ArcGIS™ of ESRI™). The resulting vector layer was analyzed in the GIS with respect to the latitudinal distribution of the depressions. All MOC-NA images available for the study region were examined for an analysis of permafrost degradation features, as they provide a very high spatial resolution of down to 1.6 m/pixel. Topographic information was derived from individual tracks of the Mars Orbiter Laser Altimeter (MOLA). Wherever applicable, depths and sizes of individual depressions were measured using standard ISIS (Integrated Software for Imagers and Spectrometers) routines. All data sets were processed in sinusoidal projections with a center longitude of 82.5°E using the officially adopted Mars IAU 2000 reference ellipsoid.

4. Results

4.1. Morphology of Landforms

[14] In general, the surface consists of a smooth material (as seen in images with low spatial resolution) with an albedo ranging between 0.14 in spring and summer and 0.19 in autumn and winter, and a mean summer-time thermal inertia of ~259, as derived from Thermal Emission Spectrometer (TES) data. MOC-NA images show several landforms that are typical for the study region (Figure 3). The material is almost completely free of fresh impact craters. Large depressions (diameters of several kilometers) are observed in which the mantling material is completely removed and the cratered floor of the underlying substrate is exposed (Figures 3a and 3b). MOLA tracks indicate a depth of ~80 m for the depression shown in Figure 3a. Since the floor of the depression shows several large craters, we assume that it corresponds to older, underlying basement material, most probably the Vastitas Borealis Formation [*Tanaka et al.*, 2005]. The depth of the depression therefore corresponds to the thickness of the mantle. The depressions are asymmetric in shape: Steep, north-facing scarps mark the southern margins of the depressions, while the northern margins (i.e., south-facing slopes) display a gently sloping surface of the bordering mantling deposit (Figures 3a and 3b). This asymmetry of the southern and northern slope is also confirmed by MOLA traverses across the depressions (Figure 4). The slopes of the southern scarp are around 5° in contrast to the more gradually rising northern margin with slopes up to ~2°. However, the slope of the southern scarp can be assumed higher than 5°. First, the scarp appears in the image data much steeper, and second small-scale slopes are smoothened due to the MOLA shot footprint of ~150 m as well as the spacing of ~300 m between the individual shots. Smaller depressions on the mantle (diameters of several hundred meters), whose depth is less than the thickness of the mantle, have a scalloped appearance and mostly display the same asymmetry as the larger ones, with steep N-facing scarps (Figure 3c). These steep margins are often arcuate-shaped, and show terraces or stepped profiles in downslope direction (Figure 3c). Where the mantle is still intact, it is characterized by polygonal fracture patterns (Figures 3c–3e). The diameter of the polygons is in the range of typically 10 m to 40 m (as seen in MOC images); however, a recent image of the High Resolution Imaging Science Experiment (HiRISE image TRA_000823_1720_RED; 25 cm/pixel in map projection, located at 46°N and 92°E) shows that there are polygons inside the scalloped depressions that have even smaller diameters of ≤10 m. The fact that the polygons inside the scalloped depressions have a distinctly different size distri-

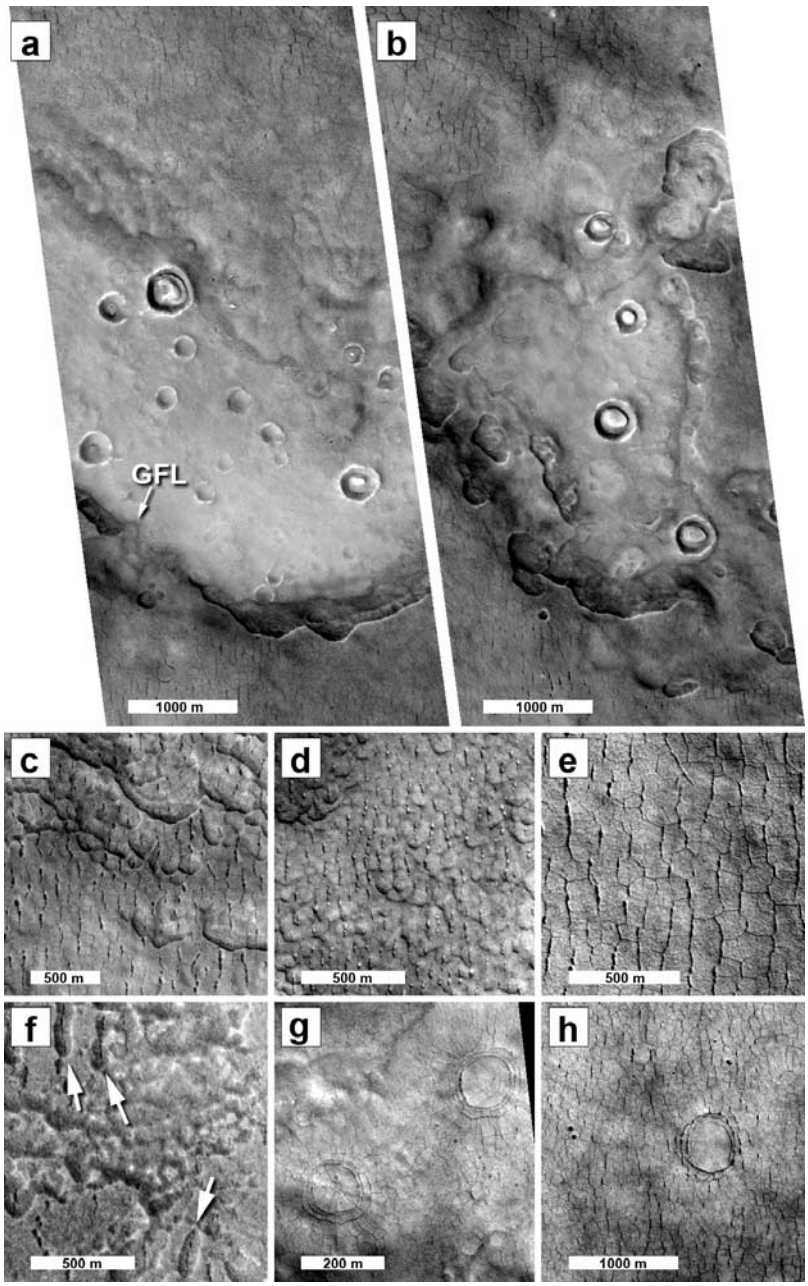

Figure 3. Examples of landforms in western Utopia Planitia. (a) Asymmetric topographic depression with steep southern scarp and more gradually rising northern margin. The floor of the depression displays impact craters, which are partly filled by layered material. The mantling material is characterized by polygonal terrain. MOLA track (ap198261) shows that the mantling material is about 80 m thick. The degraded appearance of the southern scarp in the bottom left part of the image might indicate a gelifluction lobe (GFL). MOC E04-01564, center at 41.46°N, 82.92°E. (b) Very similar asymmetric depression, with steep southern and gently rising northern margin. MOC E04-01564, center at 42.08°N, 82.81°E. (c) Polygonal terrain with preferred N-S orientation of pits along cracks. Asymmetric (''scalloped'') small depressions have steep north-facing scarps (compare with Figures 3a and 3b). MOC R11-00336, center at 45.47°N and 81.1°E. (d) Similar to Figure 3c. MOC E11-02077, center at 45.4°N and 81.44°E. (e) Uniform polygons with preferred N-S orientation. MOC M04-02704, center at 44.08°N, 84.15°E. (f) Interior of 8.8-km impact crater. Note the N-S-oriented cracks, which are bounded by U-shaped troughs (arrows in top left and bottom right parts of image). See text for details. MOC R17-00802, center at 47.62°N and 82.57°E. (g) Polygonal pattern locally modified into concentric and radial pattern. The circular cracks in the mantling material might have formed by differential compaction (see *Buczkowski and Cooke* [2004], although these authors describe much larger craters), which creates a zone of structural weakness over crater rims. MOC R05-00393, center at 42.02°N and 80.95°E. (h) Similar as in Figure 3g, concentric cracks might indicate position of mantled impact crater. MOC E04-01564, center at 41.63°N, 82.89°E.

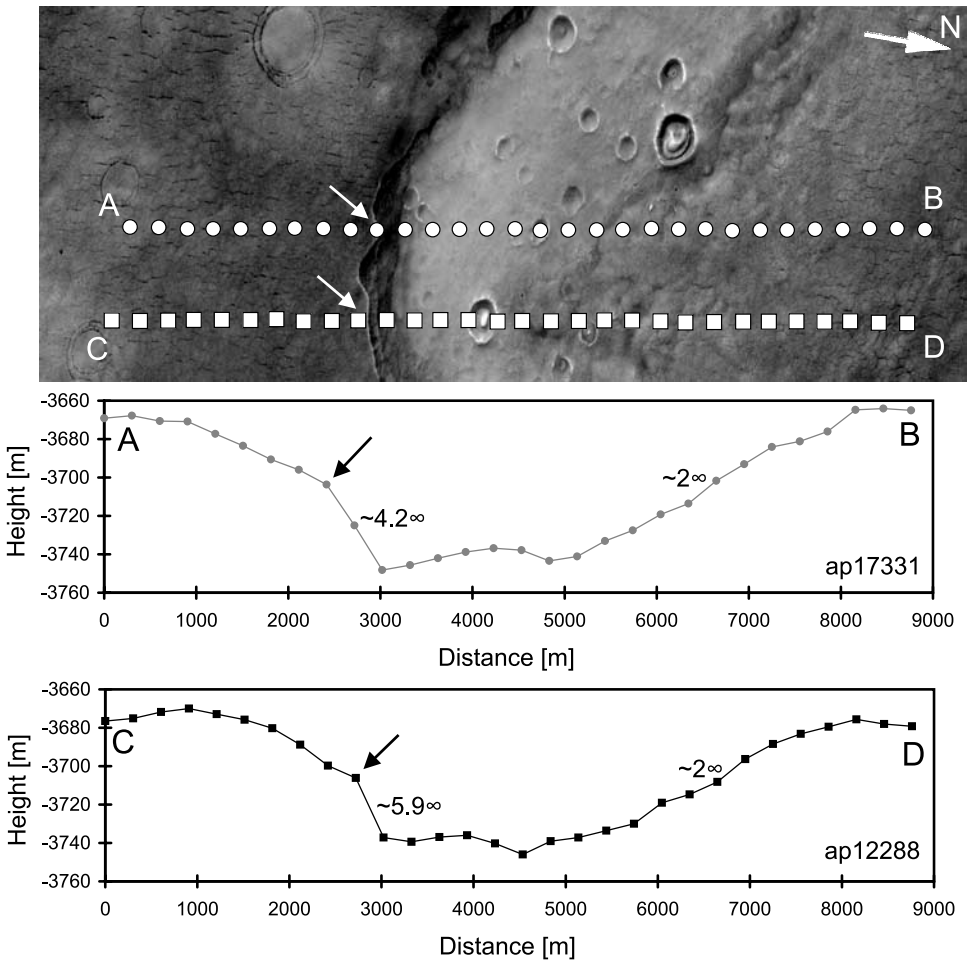

Figure 4. Two MOLA transects (ap17331 and ap12288) across a depression (MOC image E04-01564 at 41.46°N, 82.92°E; image height is 3.19 km). The top of the steeper southern scarp is labeled in the image and in the graphs with arrows. The slopes of the southern scarp are around 5°, in contrast to the more gradually rising northern margin with slopes up to ~2°.

bution than those immediately adjacent, but outside, attests different polygon generations and that the polygon formation was (still) active after the formation of the depressions. The HiRISE image also shows a large number of blocks with a maximum size of ~1 m in plan view. They seem to be uniformly distributed over the mantle, and the blocks seem to be part of the mantle, not a product of later transport and deposition. The cracks that delineate the polygon areas show a more pronounced development in N-S or NNE-SSW direction, and smaller pits are aligned along the N-S trending cracks (Figures 3c and 3e). At several locations, the N-S-trending cracks are bordered by U-shaped troughs (Figure 3f). Concentric and radial patterns mark the locations of impact craters or topographic lows in general that are buried by the mantling material (Figures 3g and 3h).

4.2. Distribution of Degradation

[15] We mapped the distribution of the large depressions (Figures 3a and 3b) in the area of 40–50°N and 80–85°E (Figure 5). Images display a varying degree of degradation, which seems to be dependent on latitude. In the northern part of the study region, the surface is smooth on a scale of hundreds of meters and displays the "basketball" surface texture described by *Kreslavsky and Head* [2000] and *Mustard et al.* [2001] (Figures 5a and 5b). This texture is typical for the mantling deposit that covers much of the high latitude-terrain on Mars. In the central section, the surface is cut by the scalloped depressions described in section 4.1 (Figures 5c and 5e). In the southern part of the study area, the mantling deposit is completely removed over large areas, revealing underlying and exhumed craters. In these craters, remnants of the mantling deposits show a subhorizontal layer geometry (Figures 5e and 5f). The percentage of the total surface covered by these depressions amounts to 24% of the study area (Figure 6). Toward the south of the study region, the depressions seem to be larger in extent (Figure 7) and their floors are populated by an abundance of small impact craters.

[16] Topographic measurements of the depressions using single MOLA tracks show that their depth is increasing toward the equator (Figure 8). Near 50°N, depressions have a depth of 10 m, while the depths increase approximately linear to ~100 m near 40°N. This suggests that in the depressions in the more northern latitudes the mantling is not completely removed. Another explanation could be a nonuniform latitudinal deposition of the mantling. Although some small depressions in the northern latitudes of the study

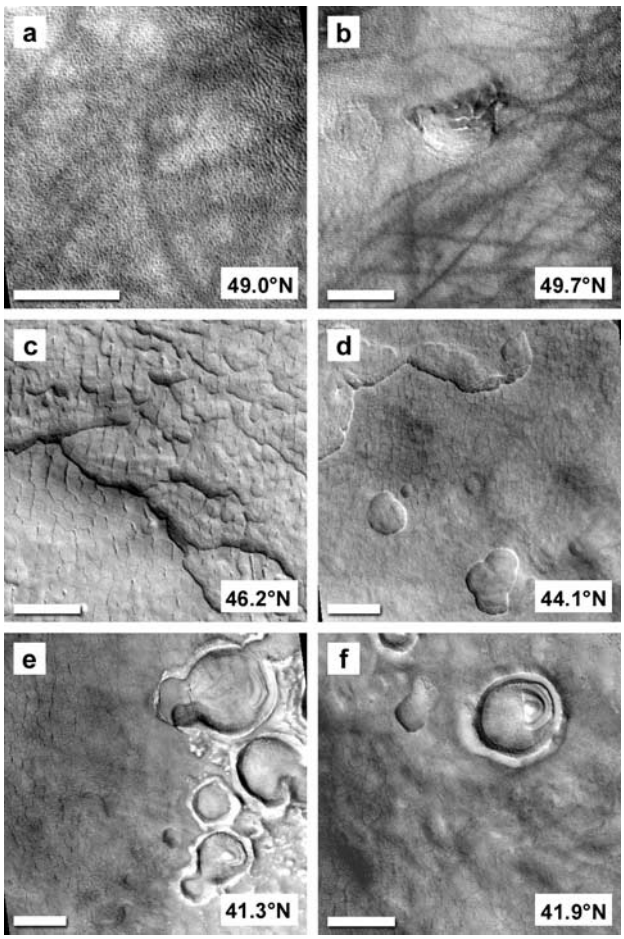

Figure 5. Latitude-dependent degradation features in western Utopia Planitia. Two typical examples are shown for the northern, middle, and southern parts of the study area, respectively. They show a gradual increase of the degradation intensity toward the south. The northern two examples (Figures 5a and 5b) exhibit a surface that lacks depressions and is characterized by the ''basketball terrain'' described by *Mustard et al.* [2001]. The origin of the hill in Figure 5b is unknown. In the center of the study area (Figures 5c and 5d), scalloped depressions cut the surface, which is also dissected by polygonal cracks. The surface in the southern part of the study area (Figures 5e and 5f) is only partly covered by the mantling deposit with the polygonal cracks, whereas the remaining parts reveal underlying and exhumed craters with subhorizontally layered remnants of the mantle. (a) Detail of MOC image M03-05440. (b) Detail of MOC R04-02303. (c) Detail of MOC R11-00336. (d) Detail of MOC E05-03354. (e) Detail of MOC E04-01564. (f) Detail of MOC R05-00393. In all images, white scale bars represent 500 m and north is up.

region suggest that the mantling is not completely removed, high-resolution imagery cannot resolve details of the basement. Therefore we cannot exclude this possibility.

5. Discussion

[17] The distribution of the mapped depressions displays a clear latitude-dependence. The ratio of the depression area to the total area increases toward south. We interpret this as evidence for a climatically controlled process, since other possible factors influencing the formation of depressions as slope gradient, relief of underlying materials, etc. do not seem to change significantly over the study area. The most plausible explanation might be the increased insolation and

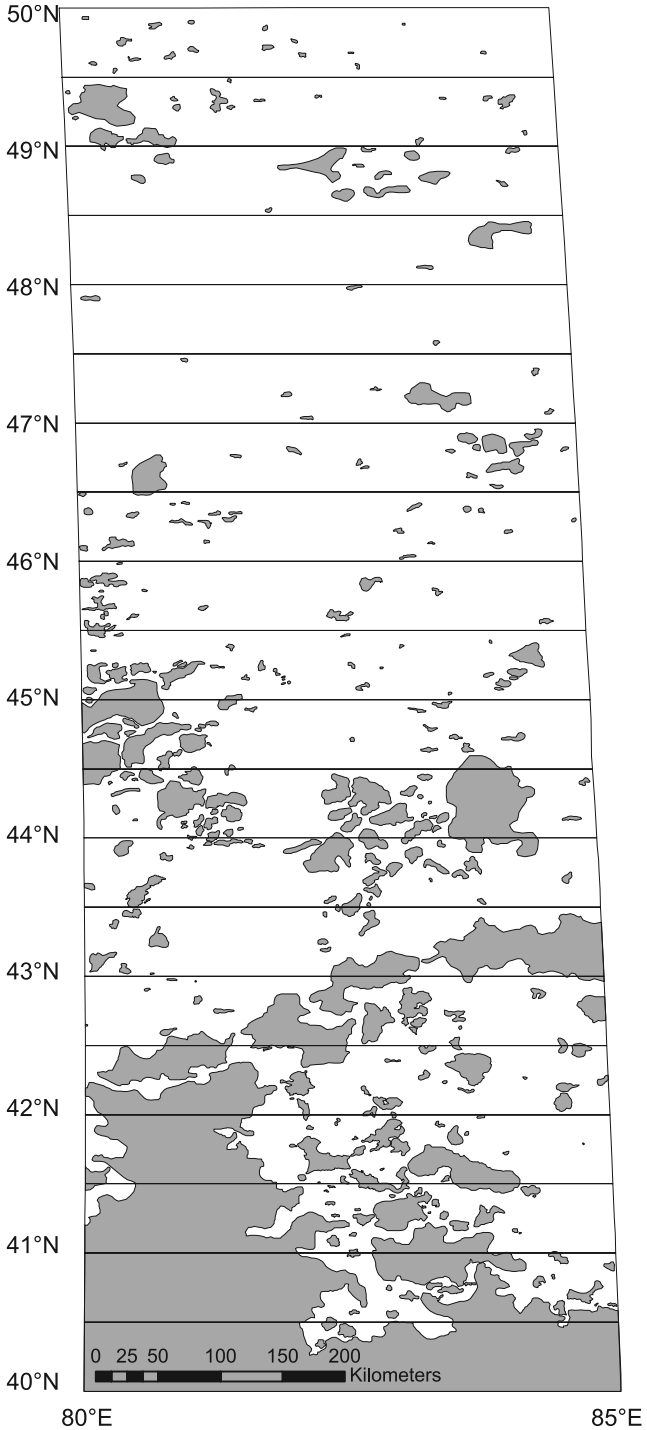

Figure 6. GIS-based map of topographic depressions (gray areas) in mantling material. Our results indicate an increasing area of depressions (= increasing degradation) from north to south, possibly indicating a climatic control of the degradation process.

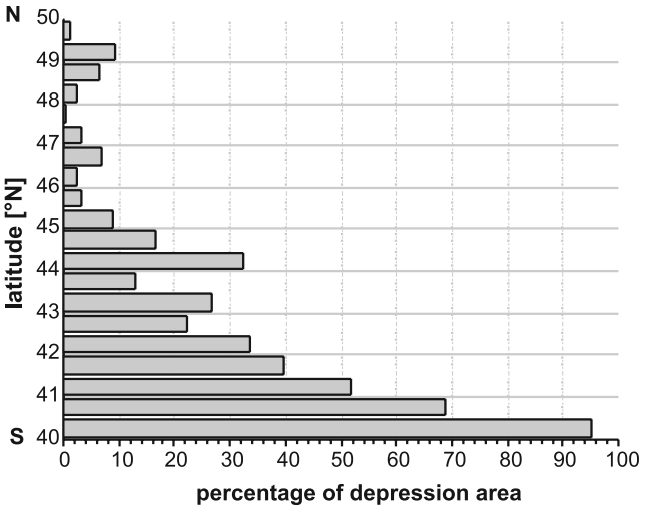

Figure 7. Latitude versus percentage of depression areas.

the higher temperatures in the south. The small-scale topography of the depressions supports our notion. The insolation from southern directions could be responsible for the asymmetric development of scalloped depressions: The S-facing slopes receive more solar energy and therefore are warmer and subject to enhanced ice sublimation. This leads to a loss of cohesion, since the ice is a major cementing factor, and the material cannot maintain steep slopes. In contrast, the N-facing slopes are protected from intense insolation, the pore ice is more stable, and the material is strong enough to maintain steep slopes. It is known from terrestrial snow surfaces that slightly differently oriented parts of the surface receive different amounts of insolation, so that small irregularities of the snow relief can become more and more accentuated [*Knight*, 1999, p. 65]. The effect of the direct illumination by the sun on snow ablation can also be observed on suncups. *Post and LaChapelle* [1971] noted that north walls of suncups on the northern hemisphere (i.e., south-facing walls) melt away faster, and ascribed this to the enhanced solar radiation. Other factors being equal, south-facing walls in the northern hemisphere will experience the most ablation [see also *Rhodes et al.*, 1987]. Further support for this explanation comes from the observation, that depressions with a similar asymmetry, but reversed sense are observed in the southern hemisphere, where *Plescia* [2003] attributed their asymmetry to solar heating. A similar trend of insolation-controlled growth of thermokarst is observed in permafrost regions of the Qinghai-Tibet Plateau, where the retrogressive extension of slope failures is higher in south-facing slopes than in north-facing slopes [*Niu et al.*, 2005]. The initial formation of a depression might have been triggered by eolian activity, since the alignment of small pits (that were proposed to act as nucleation points for the formation of larger depressions) is consistent with the prevailing wind direction [*Soare et al.*, 2005b]. However, the almost complete lack of eolian dunes suggests that eolian erosion is not the major process for the removal of the material.

[18] Although the Utopia population of possible thermal contraction patterns is approximately situated in the main northern hemispheric belt of polygonal features it is different with respect to other landforms observed in the northern hemisphere. The distribution of Utopia small-scaled polygons (UP) forms an isolated population that is slightly offset toward the south from the main band and is centered around 42°, reaching a southernmost limit of 35°. The east-west extent of the UP ranges from 57°E–101°E. The study area (80°E–85°E, 40°N–50°N) represents a subset of this area that is approximately centered in the UP distribution. The UP population has been excluded from the global mapping of polygonal thermal contraction analogues by *Mangold et al.* [2004] due to its possible relationship to impact cratering in the vicinity. We do not follow this recommendation as their morphologies and sizes are comparable to similar polygons and their association to landforms indicative of permafrost is too close to be ignored.

[19] As of MOC release S10, 60% of all observation in the UP study area show polygonal fracture patterns with a dense distribution between 40°N–45°N and almost no occurrences north of 45°N. They are clearly observed in image data with a pixel scale of 1.6 m/pixel to 6.5 m/pixel. The diameter sizes of polygons range from 50 m to 160 m in general with a maximum between 60 m to 110 m and a clear peak in the 95–105 m class bin containing 15% of all observations.

[20] Polygons are generally oriented in north-south direction with well pronounced north-south trending polygon troughs reaching a width of up to 10 m, and are less pronounced in east-west direction. Areas north of 45°N that are covered by dust or that have undergone substantial erosion only show relics of north-south trending troughs. Characteristic trough-widening and pits are almost only found on north-south trending troughs. The origin of the more pronounced width and depth of the north-south-trending cracks is unknown. A possible cause could be the prevailing wind direction during the early summer season, when surface temperatures and, accordingly, sublimation rates reach their maximum. During the time period of highest surface temperatures (240 K at LS = 100–110°), the wind direction is from SSE (azimuth, as measured clockwise from north: ~180–195°; Figure 9). This direction is perfectly parallel with the preferential orientation of the more pronounced cracks. A possible explanation would

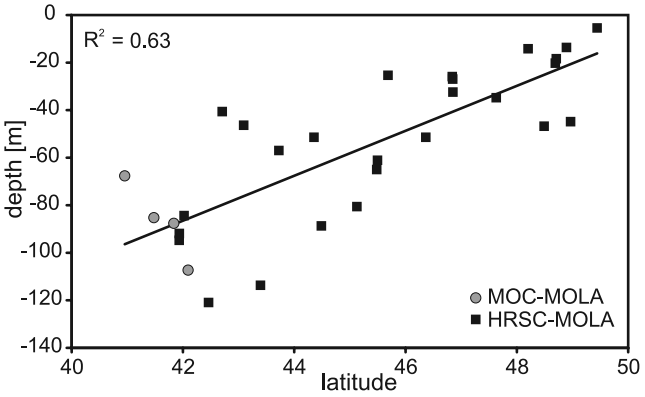

Figure 8. Depth of depressions versus latitude. The depth increases toward the equator, possibly indicating a climatic control of the degradation process.

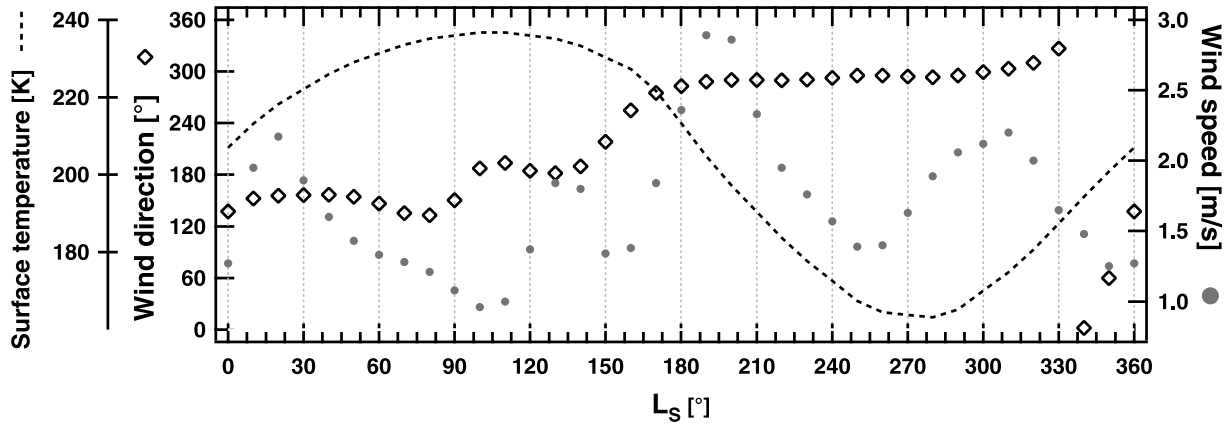

Figure 9. Wind direction, wind speed, and surface temperatures over a full Martian year at the center of the study area at 82.5°E and 45°N. During the period of the highest surface temperatures (early summer; LS = ~100–110°), when sublimation rates are expected to be at their maximum, the wind comes from south to SSW (azimuth 180° – 195°). This is exactly parallel to the dominant crack orientation (e.g., Figures 3c–3e). An increased energy transfer into N-S-trending cracks might cause enhanced sublimation and degradation of their walls (data were derived from a General Circulation Model available at http://www-mars.lmd.jussieu.fr/ [e.g., *Forget et al.*, 1999] and were kindly provided by Francois Forget and Ehouarn Millour).

be an enhanced degradation of N-S-trending cracks due to an increased energy transfer by warm winds to their walls, leading to increased sublimation. However, other possibilities exist, such as structural control from bending forces originating at the center of the Utopia basin [*Yoshikawa*, 2003]. On featureless plains, polygon shapes are irregularly distributed, some being hexagonal, some being rectangular. They are frequently oriented along scarps or in substrate that buries possible impact-crater structures.

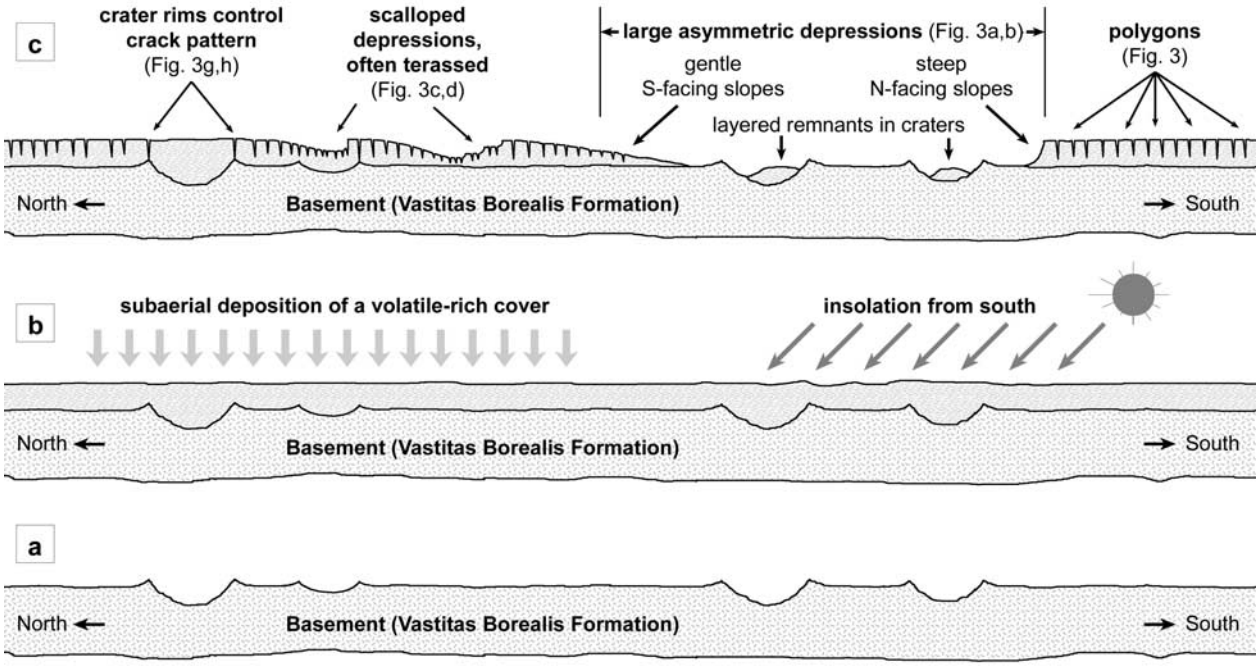

Figure 10. Schematic model for landscape genesis in western Utopia Planitia. (a) Cratered basement, probably the Vastitas Borealis Formation [*Tanaka et al.*, 2005]. (b) Subaerial deposition of a volatile-rich mantling material (ice-dust mixture). Insolation comes mainly from southern directions. (c) The sublimation of pore ice causes volume loss and the formation of polygonal crack patterns, smaller scalloped depressions, and larger depressions which affect the entire thickness of the mantling material. The depressions appear asymmetric in cross-sectional N-S profiles, since the increased insolation on S-facing slopes leads to enhanced disintegration of the ice-dust mixture and to slope failure.

[21] Size, shape and morphometric parameters of the studied depressions at Utopia Planitia are apparently very similar to terrestrial thermokarst depressions in NE Siberian ice-rich permafrost deposits. In the NE Siberian periglacial, the coexistence of thermokarst depressions with polygonal ground in the surroundings is closely connected to the (former) presence of ice-rich permafrost. These Yedoma deposits were formed under cold-climatic continental conditions, relatively independent from sedimentological facies. The Yedoma-thermokarst assemblage could be considered as a fairly good analogy to the supposed volatile-rich mantle and its basin structures in Utopia Planitia on Mars. On Earth, the climatically controlled degradation of the ice-rich permafrost deposits during the Early Holocene resulted in characteristic negative landforms, which dominate the present-day landscapes in NE Siberia and other Arctic lowlands.

6. Conclusions

[22] On the base of our observations, we propose a schematic model of landscape genesis for western Utopia Planitia (Figure 10). It involves the subaerial deposition of a stack of ice-rich sedimentary layers on a cratered basement and its postsedimentary permafrost degradation. The thickness of the sediments is in the order of tens of meters. From the almost total lack of impact craters we conclude that the sedimentation of this material occurred very late in Martian history (very Late Amazonian). This material was subsequently degraded. The dominant degradation process was most probably the sublimation of ice in the layers, leading to volume loss and surface collapse. The deposition and subsequent climate-controlled degradation of a volatile-rich deposit implies a changing climate very late in Martian history. The close similarity of the assemblage of Martian landforms to terrestrial analogies in NE Siberia suggests that no unusual surface processes are needed to explain the most recent landscape evolution in western Utopia Planitia.

[23] **Acknowledgments.** We gratefully appreciate the efforts of the MOC, HRSC, THEMIS, MOLA, and HiRISE Teams, who made their data products available to the public. Discussions with Alexandra Lefort helped a lot in writing this manuscript. We thank Francois Forget and Ehouarn Millour for kindly providing GCM data for our study area.

References

Black, R. F. (1976), Periglacial features indicative of permafrost: Ice and soil wedges, *Quat. Res.*, *6*, 3–26.

Buczkowski, D. L., and M. L. Cooke (2004), Formation of double-ring circular grabens due to volumetric compaction over buried impact craters: Implications for thickness and nature of cover material in Utopia Planitia, Mars, *J. Geophys. Res.*, *109*, E02006, doi:10.1029/2003JE002144.

Carr, M. H., and G. G. Schaber (1977), Martian permafrost features, *J. Geophys. Res.*, *82*, 4039–4054.

Costard, F. M., and V. R. Baker (2001), Thermokarst landforms and processes in Ares Vallis, Mars, *Geomorphology*, *37*, 289–301.

Costard, F. M., and J. S. Kargel (1995), Outwash plains and thermokarst on Mars, *Icarus*, *114*, 93–112.

Forget, F., F. Hourdin, R. Fournier, C. Hourdin, O. Talagrand, M. Collins, S. R. Lewis, P. L. Read, and J.-P. Huot (1999), Improved general circulation models of the Martian atmosphere from the surface to above 80 km, *J. Geophys. Res.*, *104*(E10), 24,155–24,176.

French, H. M. (1996), *The Periglacial Environment*, 341 pp., Addison-Wesley, Boston, Mass.

Gatto, L. W., and D. M. Anderson (1975), Alaskan thermokarst terrain and possible Martian analog, *Science*, *188*, 255–257.

Grosse, G., L. Schirrmeister, V. V. Kunitsky, and H.-W. Hubberten (2005), The use of CORONA images in remote sensing of periglacial geomorphology: An illustration from the NE Siberian coast, *Permafrost Periglacial Processes*, *16*, 163–172.

Grosse, G., L. Schirrmeister, and T. J. Malthus (2006), Application of Landsat-7 satellite data and a DEM for the quantification of thermokarst-affected terrain types in the periglacial Lena-Anabar coastal lowland, *Pol. Res.*, *25*, 51–67.

Grosse, G., L. Schirrmeister, C. Siegert, V. V. Kunitsky, E. A. Slagoda, A. A. Andreev, and A. Y. Dereviagyn (2007), Geological and geomorphological evolution of a sedimentary periglacial landscape in northeast Siberia during the Late Quaternary, *Geomorphology*, *86*(1/2), 25–51, doi:10.1016/j.geomorph.2006.08.005.

Hiesinger, H., and J. W. Head (2000), Characteristics and origin of polygonal terrain in southern Utopia Planitia, Mars: Results from Mars Orbiter Laser Altimeter and Mars Orbiter Camera data, *J. Geophys. Res.*, *105*, 11,999–12,022.

Hinkel, K. M., W. R. Eisner, J. G. Bockheim, F. E. Nelson, K. M. Peterson, and X. Dai (2003), Spatial extent, age, and carbon stocks in drained thaw lake basins on the Barrow Peninsula, Alaska, *Arctic Antarct. Alpine Res.*, *35*(3), 291–300.

Kargel, J. S., and R. G. Strom (1992), Ancient glaciation on Mars, *Geology*, *20*, 3–7.

Knight, P. G. (1999), *Glaciers*, 261 pp., Stanley Thornes, Cheltenham, UK.

Kossacki, K. J., and W. J. Markiewicz (2002), Martian seasonal CO_2 ice in polygonal troughs in the southern polar region: Role of the distribution of subsurface H_2O ice, *Icarus*, *160*, 73–85.

Kreslavsky, M. A., and J. W. Head (2000), Kilometer-scale roughness of Mars' surface: Results from MOLA data analysis, *J. Geophys. Res.*, *105*, 26,695–26,712.

Kreslavsky, M. A., and J. W. Head (2002), Fate of outflow channel effluents in the northern lowlands of Mars: The Vastitas Borealis Formation as a sublimation residue from frozen ponded bodies of water, *J. Geophys. Res.*, *107*(E12), 5121, doi:10.1029/2001JE001831.

Kuzmin, R. O. (1983), *Cryolithosphere of Mars*, 144 pp., Nauka, Moscow.

Kuzmin, R. O., and E. V. Zabalueva (2003), Polygonal terrains on Mars: Preliminary results of global mapping of their spatial distribution, *Lunar Planet. Sci.*, *XXXIV*, abstract 1912.

Kuzmin, R. O., E. D. Yershow, I. A. Komarow, A. H. Kozlov, and V. S. Isaev (2002), The comparative morphometric analysis of polygonal terrains on Mars and the Earth high latitude areas, *Lunar Planet. Sci.*, *XXXIII*, abstract 2030.

Lachenbruch, A. H. (1962), Mechanics of thermal contraction cracks and ice-wedge polygons in permafrost, *Spec. Pap. Geol. Soc. Am.*, *70*, 68 pp.

Lachenbruch, A. H. (1966), Contraction theory of ice-wedge polygons: A qualitative discussion, in *Proceedings Permafrost International Conference, Lafayette, Indiana, November 1963*, *Publ. 1287*, pp. 63–71, U. S. Natl. Acad. of Sci., Washington, D. C.

Lucchitta, B. K. (1981), Mars and Earth—Comparison of cold-climate features, *Icarus*, *45*, 264–303.

Lucchitta, B. K. (1983), Permafrost on Mars: Polygonally fractured ground, in *Proceedings of the 4th International Conference on Permafrost*, Nat. Acad. Press, Washington, D. C.

Lucchitta, B. K. (1985), Geomorphologic evidence for ground ice on Mars, in *Ices in the Solar System*, edited by J. Klinger et al., pp. 583–604, Springer, New York.

Mangold, N. (2005), High latitude patterned grounds on Mars: Classification, distribution and climatic control, *Icarus*, *174*, 336–359.

Mangold, N., S. Maurice, W. C. Feldman, F. Costard, and F. Forget (2004), Spatial relationships between patterned ground and ground ice detected by the Neutron Spectrometer on Mars, *J. Geophys. Res.*, *109*, E08001, doi:10.1029/2004JE002235.

Mellon, M. T. (1997), Small-scale polygonal features on Mars: Seasonal thermal contraction cracks in permafrost, *J. Geophys. Res.*, *102*, 25,617–25,628.

Mustard, J. F., C. D. Cooper, and M. K. Rifkin (2001), Evidence for recent climate change on Mars from the identification of youthful near-surface ground ice, *Nature*, *412*, 411–414.

Mutch, T. A., R. E. Arvidson, E. A. Guinness, A. B. Binder, and E. C. Morris (1977), The geology of the Viking Lander 2 site, *J. Geophys. Res.*, *82*, 4452–4467.

Niu, F., G. Cheng, W. Ni, and D. Jin (2005), Engineering-related slope failure in permafrost regions of the Qinghai-Tibet Plateau, *Cold Regions Sci. Technol.*, *42*, 215–225.

Paige, D. A. (1992), The thermal stability of near-surface ground ice on Mars, *Nature*, *356*, 43–45.

Piqueux, S., S. Byrne, and M. I. Richardson (2003), Polygonal landforms at the South Pole and implications for exposed water ice, in *Sixth International Conference on Mars*, p. 3275, Lunar and Planet. Inst., Houston, Tex.

Plescia, J. B. (2003), Amphitrites-Peneus Paterae/Malea Planum geology, *Lunar Planet. Sci.*, *XXXIV*, abstract 1478.

Post, A., and E. R. LaChapelle (1971), *Glacier Ice*, Univ. of Wash. Press, Seattle.

Rhodes, J. J., R. L. Armstrong, and S. G. Warren (1987), Mode of formation of "ablation hollows" controlled by dirt content of snow, *J. Glaciol.*, *33*(114), 135–139.

Schirrmeister, L., C. Siegert, T. Kuznetsova, S. Kuzmina, A. A. Andreev, F. Kienast, H. Meyer, and A. A. Bobrov (2002), Paleoenvironmental and paleoclimatic records from permafrost deposits in the Arctic region of Northern Siberia, *Quat. Int.*, *89*, 97–118.

Seibert, N. M., and J. S. Kargel (2001), Small-scale Martian polygonal terrain: Implications for liquid surface water, *Geophys. Res. Lett.*, *28*, 899–902.

Sharp, R. P. (1973), Mars: Fretted and chaotic terrain, *J. Geophys. Res.*, *78*, 4073–4083.

Soare, R. J., D. M. Burr, and J. M. Wan Bun Tseung (2005a), Possible pingos and a periglacial landscape in northwest Utopia Planitia, *Icarus*, *174*, 373–382.

Soare, R. J., J. M. Wan Bun Tseung, and C. Peloquin (2005b), Possible thermokarst and alas formation in Utopia Planitia, Mars, *Lunar Planet. Sci.*, *XXXVI*, abstract 1103.

Soderblom, L. A., M. C. Malin, J. A. Cutts, and B. C. Murray (1973), Mariner 9 observations of the surface of Mars in the north polar region, *J. Geophys. Res.*, *78*, 4197–4210.

Squyres, S. W. (1978), Martian fretted terrain—Flow of erosional debris, *Icarus*, *34*, 600–613.

Squyres, S. W. (1979), The distribution of lobate debris aprons and similar flows on Mars, *J. Geophys. Res.*, *84*, 8087–8096.

Squyres, S. W., and M. H. Carr (1986), Geomorphic evidence for the distribution of ground ice on Mars, *Science*, *231*, 249–252.

Squyres, S. W., S. M. Clifford, R. O. Kuzmin, J. R. Zimbelman, and F. M. Costard (1992), Ice in the Martian regolith, in *Mars*, edited by H. H. Kieffer et al., pp. 523–554, Univ. of Ariz. Press, Tucson.

Tanaka, K. L., J. A. Skinner, and T. M. Hare (2005), Geologic map of the northern plains of Mars, scale 1:15,000,000, *U. S. Geol. Surv. Sci. Invest.*, *Map 2888*.

Theilig, E., and R. Greeley (1979), Plains and channels in the Lunae Planum-Chryse Planitia region of Mars, *J. Geophys. Res.*, *84*, 7994–8010.

van Everdingen, R. O. (Ed.) (2005), *Multi-Language Glossary of Permafrost and Related Ground-Ice Terms, International Permafrost Association*, Univ. of Calgary, Calgary, Canada. (Available at http://nsidc.org/fgdc/glossary)

van Gasselt, S., D. Reiss, and R. Jaumann (2003), Distribution and morphology of polygons, south polar region, Mars, in *Third International Conference on Mars Polar Science and Exploration*, Abstract 8088, Lunar and Planet. Inst., Houston, Tex.

van Gasselt, S., D. Reiss, A. K. Thorpe, and G. Neukum (2005), Seasonal variations of polygonal thermal contraction crack patterns in a south polar trough, Mars, *J. Geophys. Res.*, *110*, E08002, doi:10.1029/2004JE002385.

Yershov, E. D. (2004), *General Geocryology* (*Obshchaya Geokriologiya*), Studies in Polar Research, 580 pp., Cambridge Univ. Press, New York.

Yoshikawa, K. (2000), Contraction cracking and ice wedge polygons in Mars, in *Second International Conference on Mars Polar Science and Exploration*, Abstract 4045, Lunar and Planet. Inst., Houston, Tex.

Yoshikawa, K. (2003), Origin of the polygons and the thickness of Vastitas Borealis Formation in Western Utopia Planitia on Mars, *Geophys. Res. Lett.*, *30*(12), 1603, doi:10.1029/2003GL017165.

Zent, A. P., F. P. Fanale, J. R. Salvail, and S. E. Postawko (1986), Distribution and state of H_2O in the high-latitude shallow subsurface of Mars, *Icarus*, *67*, 19–36.

Zhang, T., R. G. Barry, K. Knowles, J. A. Heginbottom, and J. Brown (1999), Statistics and characteristics of permafrost and ground ice distribution in the Northern Hemisphere, *Pol. Geogr.*, *23*, 132–154.

G. Grosse, Geophysical Institute, University of Alaska Fairbanks, 903 Koyukuk Drive, Fairbanks, AK 99775-7320, USA.

E. Hauber, Institute of Planetary Research, German Aerospace Center (DLR), Rutherfordstr. 2, D-12489 Berlin, Germany.

A. Morgenstern and L. Schirrmeister, Alfred Wegener Institute for Polar and Marine Research, Research Unit Potsdam, Telegrafenberg A 43, D-14401 Potsdam, Germany. (anne.morgenstern@awi.de)

D. Reiss, Institut für Planetologie, Westfälische Wilhelms-Universität Münster, Wilhelm-Klemm-Str. 10, D-48149 Münster, Germany.

S. van Gasselt, Institute for Geosciences, Planetology and Remote Sensing, Freie Universitaet Berlin, Malteserstr. 74-100, D-12249 Berlin, Germany.